Journal of Engineering Science and Technology
Vol. 13, No. 11 (2018) 3821 - 3839

AUTOMATIC LIVER SEGMENTATION FROM CT SCANS USING INTENSITY ANALYSIS AND LEVEL-SET ACTIVE CONTOURS

OMAR IBRAHIM ALIRR, ASHRANI AIZZUDDIN ABD. RAHNI*

Centre for Integrated Systems Engineering and Advanced Technologies (Integra),
Faculty of Engineering and Built Environment, Universiti Kebangsaan Malaysia,
43600 Bangi, Selangor, Malaysia
*Corresponding Author: ashrani@ukm.edu.my

Abstract

Liver segmentation from CT scans is still a challenging task due to the liver characteristics in terms of shape and intensity variability. In this work, we propose an automatic segmentation method of the liver from CT data sets. The framework consists of three main steps: liver shape model localization, liver intensity range estimation and localized active contouring. We proposed an adaptive multiple thresholding technique to estimate the range of the liver intensities. First, multiple thresholding is used to extract the dense tissue from the whole CT scan. A localization step is then used to find the approximate location of the liver in the CT scan, to localize a constructed mean liver shape model. A liver intensity-range estimation step is then applied within the localized shape model ROI. The localized shape model and the estimated liver intensity range are used to build the initial mask. A level set based active contour algorithm is used to deform the initial mask to the liver boundaries in the CT scan. The proposed method was evaluated on two public data sets: SLIVER07 and 3D-IRCAD. The experiments showed that the proposed method is able to segment to liver in all CT scans in the two data sets accurately.

Keywords: Automatic segmentation, Intensity analysis, Localized contouring, Multiple thresholding.

1. Introduction

Liver cancer considered as one of cancer diseases that cause high number of deaths every year. Liver cancer treatments can be generally divided into three categories: surgical resection, liver transplantation and minimally invasive treatments such as ablation. However, all these kinds of procedures require accurate diagnosis and planning [1].

Medical imaging using computed tomography (CT) scans play an important role in liver cancer diagnosis. It is considered as one of the non-invasive diagnosis tools for hepatic diseases. It is the most commonly used imaging techniques for liver cancer diagnosis, since it gives accurate anatomical information about the abdominal organs in the human body [2].

Liver organ segmentation from CT scans is an important step in medical imaging applications, since accurate identification of the liver anatomy helps in clinical assessment of the risks and benefits of hepatic interventions [3]. However, determination of anatomic segments of the liver manually from Computed Tomography (CT) scans in 3D is a tedious and time consuming process. Besides that, it greatly depends on the skills of the physician or doctor who perform the segmentation task. Therefore, there is a need to automate the segmentation process.

Automatic segmentation of the liver from CT scans is a challenging task because of many reasons. Low contrast and blurry edges are the main characteristics of CT images, which makes liver delineation a challenging task. This is due to neighboring tissue and organs such as the heart, spleen and kidneys having similar intensities [4]. The non-uniformity of the distribution of injected contrast media impose and additive complexity. Moreover, the liver has high variability in terms of shape and volume between different patients [5].

In this paper, we propose an automatic intensity based segmentation technique. Within our framework, a multiple thresholding method is used to extract the approximate intensity range of the liver in the CT scan. It is a challenging task, because other surrounding organs and tissue have similar intensities with the liver. The method is initialized by localizing a mean shape model of the liver in a CT image. A multiple thresholding approach is utilized based on two automatic thresholding techniques, the Otsu method and using Gaussian mixture models with expectation minimization. This multiple thresholding approach is applied in the region of interest (ROI) found using the localized liver model to find an approximate liver intensity range. This liver intensity range is then used with an active contour algorithm to segment the liver from CT scan.

Related work

Computer-aided systems have contributed significantly in the diagnosis of the liver. These systems show the anatomical structure of liver and its vessels in the form of volumetric views, giving the surgeons the ability to assess and take accurate decisions about the patient's situation within shorter period of time. Within the component of such computer aided systems, accurate segmentation of the liver from CT images arguably is the most important and challenging task [1, 6].

Many segmentation techniques have been proposed to segment the liver from CT scans, as evident from numerous reviews published [1, 6-8]. As per Luo et al. [7],

based on the image features used, we can generally divide segmentation techniques into three categories: intensity based segmentation, shape model based segmentation and texture based classification. As our work is intensity based utilizing a shape model, we limit this review to these two broad categories. We also look at hybrid techniques, which in general combine intensity-based techniques with shape models.

Intensity based techniques aim to find the intensity range of the liver organ by applying a statistical analysis on the intensities in CT scans [5, 9, 10]. The idea is to produce a binary image, based, rather directly, on the properties of the intensities present in the CT scan. Intensity based techniques can be further divided into a number of sub-categories: thresholding, clustering/classification, active contour, region growing and graph cut methods.

The simplest techniques are those based on thresholding, such as using the Otsu algorithm. Techniques that are more sophisticated are those based on clustering or classification, such as those based on Otsu, k-means or Gaussian mixture model (GMM) clustering. These are used to extract a rough segmentation of liver based on an assumed class of intensities. Clustering techniques can be combined with other methods, Foruzan et al. [5] used a semi-automated method, initialized by a manually selected slice that has the biggest cross section of the liver. They used GMM with expectation maximization (EM) to apply an adaptive threshold based on liver intensity statistics. The initial segmentation is then further refined by a geodesic active contour. However, the technique was unable to include the liver vessels within the liver segmentation, and that affects the segmentation results significantly, especially when the vessels have higher intensity values compared to liver tissue. Goryawala et al. [10] on the other hand, use the k-means algorithm to form five initial clusters, from which an initial mask is constructed for an active contour method. The authors tried to minimize human intervention by designing the initialization masks for region contouring.

Active contour methods can also be used more independently. Altarawneh et al. [11] proposed a semi-automatic level set based active contour method to segment the liver in CT images. They proposed a modified distance-regularized model to guide the contour evolution. A manually selected reference slice initializes the method, which can be the middle slice or the largest cross section of the liver. A previously segmented slice then becomes the initial contour for an adjacent slice.

Region growing methods aim to combine voxels that have similar intensity values with each other [7, 12, 13]. The most important step in these methods is seed selection, which is usually provided manually by the user [7], a region-growing rule then needs to be specified. Wang et al. [14] proposed an improved segmentation method based on three dimensional region growing method, they adopted a 18-neigbourhood 3D ROI for region growing. The seed point will grow to the 18 neighbourhood directions at the same time, so the correlation between slices can be fully utilized. In most proposed methods, the initial seed selection has high impact on the results. In general, region growing works well with homogenous liver intensities. However, under-segmentation cannot be avoided when tumors are present, especially with big tumors. Over-segmentation by connection with neighbor tissues is also a problem with region growing methods [9, 15].

Graph cut techniques are based on the idea that an image can be considered as an undirected graph. In this graph, pixels or voxels are represented as vertices, and the connections between them are represented by edges. The weight of the edges

represent the connectivity and the similarity of the vertices in terms of their intensities. Graph cut methods can be used to optimized other methods such as shape models which are explained below [16, 17]. Wu et al. [18] proposed a semiautomatic graph cut method to segment the liver and tumors. The method starts by applying low-level processing steps to generate the threshold range, which is followed by a supervoxel generation step using simple linear iterative clustering of the liver region of interest. Then the graph cut approach is applied on the seed extracted from the largest slice to segment the liver. Liao et al. [19]proposed an automatic method based on the graph cut and border marching to segment liver in CT scans. They use an intensity model and PCA regional appearance model to enhance the contrast of liver compared to the background. Then the graph cut is used based on these models and the location constrained to segment the liver in each slice iteratively.

Shape model based techniques depend on a probabilistic model that represents the variation of the shape of organs, as prior knowledge to impose constraints in an image segmentation task [18-22]. Model-based segmentation methods usually consist of two stages, the first stage is to initialize the location of the model, while the second stage is to fit the shape and appearance of the model to match closely to a desired segmentation from the image. Many statistical shape model (SSM) techniques have been reviewed [23]. Li et al. [24] proposed an automatic liver segmentation technique based on shape and appearance model to fit the liver model to the CT scan, then a simplex mesh deformation method is used to refine the segmentation result. However, since the liver has high variation in terms of shape and image intensity, the accuracy of a model based segmentation technique requires a large number of training data to be available for model construction, in order to represent this variability.

There exist a number of works, which combine shape models with intensity-based techniques. Platero et al. [16] proposed a combination of low-level operations and use of multiple probabilistic atlas for segmentation. Firstly, a probabilistic atlas is localized in the image using affine registration as an initial segmentation of the liver. This initial segmentation is the used to select additional atlases are then used in combination to generate final the segmentation result. As mentioned above, the graph cut technique is used to optimize the segmentation. Li et al. [24] localize a mean shape model of the liver mean shape model in a CT scan using thresholding and the distance transform. The localized liver mesh is then deformed to the liver surface using the graph cut method. Linguraru et al. [25] proposed a method by combining atlas registration with geodesic active contours to segment the liver in CT scans. The atlas is registered to the liver in using affine registration based on the mutual information similarity. The registered atlas is then deformed as a geodesic active contour to refine the segmentation to better follow liver boundaries.

Christ et al. proposed an automatic machine learning segmentation method using the cascaded fully conventional neural networks. The authors train and cascade two fully conventional neural networks for liver and tumor segmentation. The first FCN is trained to segment the liver as region of interest which is followed by the second FCN to segment the tumors [26].

In comparing different methods, it is important to have the same dataset for evaluation. Heimann et al. [27] made a comparative study of a group of automatic and semiautomatic segmentation techniques utilizing the same dataset and highlighted the performance of the different approaches.

2. Methodology

Liver segmentation from CT scans is a challenging task, due the similar intensities of the surrounding abdominal organs such as the spleen, heart and kidneys. In this paper, we propose a method of liver segmentation which is fully automatic, requiring no user intervention. The framework consists of five main stages as shown in Fig. 1: multiple thresholding, liver localization, liver intensity range estimation, level set based localized active contouring and post-processing. Our approach is applicable on contrast enhanced CT scans, which first undergo median filtering. These five main stages are detailed in the following subsections.

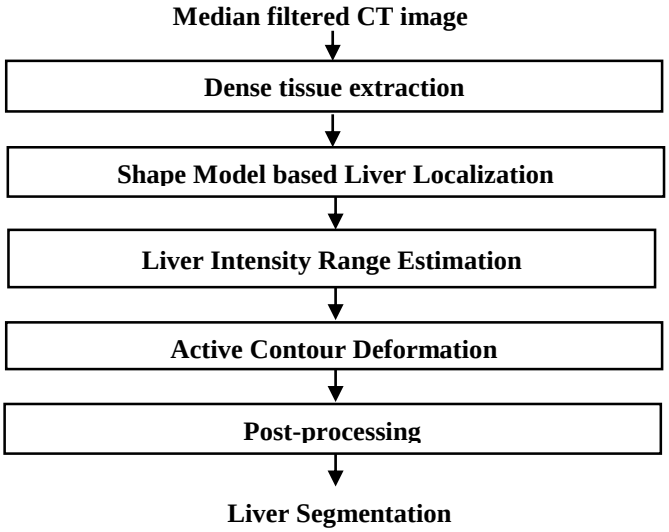

Fig. 1. Flow chart of the proposed liver segmentation approach.

2.1. Multiple thresholding: Dense tissue extraction

Thresholding is a technique for segmentation of images based on intensities at the individual pixel or voxels level. The result of thresholding is a binary image based on whether each pixel or voxel is above or below a specified threshold value, measured in intensity Hounsfield Units (HU). An example of an algorithm to specify a threshold value is the Otsu algorithm. On the other hand, clustering techniques may be considered an extension of thresholding, for example k-means or GMM based clustering [5, 10].

In our work, based on empirical results, we found that a single technique is not sufficient to cluster the main categories of body tissue from CT images, namely bones, dense tissue and soft tissue organs. Subsequently, in this work we proposed an extended thresholding technique to cluster the main categories of body tissue by finding the appropriate intensity thresholds between them. For this purpose, we used two techniques, the Otsu algorithm and Gaussian Mixture Model (GMM) with Expectation-Maximization (EM).

The Otsu algorithm is an automatic, fast and robust technique that can be used to classify data for two clusters. The measured statistical means and standard deviations at an optimal threshold guarantee the minimum within class variance (σ_w^2) between

the two classes [28], this initial optimal threshold called the global threshold (T_g), and can be measured according to the discrimination Eq. (1) as given below;

$$\sigma_w^2 = w_0(T_g)\sigma_0^2(T_g) + w_1(T_g)\sigma_1^2(T_g) \quad (1)$$

Weights w_0 and w_1 are the probabilities of the two classes. On the other hand, a Gaussian mixture model can be employed to model the intensity distribution of the liver. A linear combination of more Gaussian distributions is known as mixture of distributions. Sufficient number of Gaussians and with the appropriate means and covariances can approximate any continuous density to arbitrary accuracy. The superposition of K Gaussian densities can be represented by Eq. (2):

$$p(\mathbf{x}) = \sum_{k=1}^{K} \pi_k N(\mathbf{x}|\boldsymbol{\mu}_k, \Sigma_k) \quad (2)$$

where each Gaussian density N is a component of the mixture and has its own mean $(\boldsymbol{\mu}_k)$, covariance (Σ_k) and mixing coefficient (π_k) [29].

For the above Gaussian mixture, the aim is to maximize the likelihood function with respect to the parameters (mean and covariance). The two steps in EM algorithm aim to estimate the posterior probability, and to calculate the model parameters. The expectation maximization steps implement few steps to maximize the likelihood. It starts by initializing the means $(\boldsymbol{\mu}_\mathbf{k})$, covariances (Σ_k) and the mixing coefficient (π_k), and evaluate these initial values for likelihood. The E-step aims to evaluate the responsibilities using the current parameter values by finding the posterior probability $(\gamma(z_k))$ for data point $\mathbf{x}_n$ using Eq. (3) below [29];

$$\gamma(z_{nk}) = \frac{\pi_k N(\mathbf{x}_n|\boldsymbol{\mu}_\mathbf{k}, \Sigma_k)}{\sum_{j=1}^{K} \pi_j N(\mathbf{x}_n|\boldsymbol{\mu}_j, \Sigma_j)} \quad (3)$$

The M-step re-calculate the parameters using the current responsibilities and the following Eqs. (4) - (6);

$$\boldsymbol{\mu}_k = \frac{1}{N_k} \sum_{n=1}^{N} \gamma(z_{nk})\mathbf{x}_n \quad (4)$$

$$\Sigma_\mathrm{k} = \frac{1}{N_k} \sum_{n=1}^{N} \gamma(z_{nk})(\mathbf{x}_n - \boldsymbol{\mu}_\mathrm{k})(\mathbf{x}_n - \boldsymbol{\mu}_\mathrm{k})^\mathrm{T} \quad (5)$$

$$\pi_k = \frac{N_k}{N} \quad (6)$$

with $N_k = \sum_{n=1}^{N} \gamma(z_{nk})$

In our work and based on empirical results, we found that GMM thresholding technique showed its superiority over the Otsu method to find the proper bone threshold in the CT scan. We used GMM with EM algorithm to represent a combination of two (K=2) Gaussian mixtures, one to represent the bone intensities and the second to represent the remaining body structures.

After extracting the accurate threshold of the bone using GMM, the Otsu method is applied on the remaining body to extract the dense tissue threshold. We used Otsu thresholding multiple times on different ranges of intensities to determine the different body tissues. Figure 2 shows the steps of extracting the main body components from a CT image.

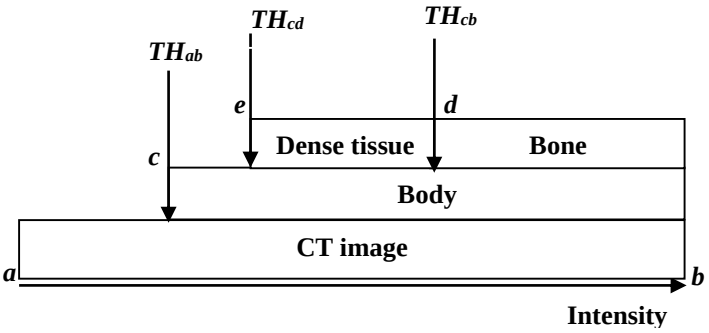

Fig. 2. Multiple thresholding process to extract the dense tissue from the whole CT scan.

The multiple thresholding process can be represented by three steps:

Step 1: Initially, the patient's body is segmented from the CT image by dividing the range of image intensities (*a*-*b*) with a threshold *c*. This threshold is found using the Otsu algorithm.

Step 2: The range of body intensities (*c*-*b*) is then divided by a second threshold *d* to separate the bones from soft tissue. For this purpose, we use the GMM with EM to find the two clusters. We found that it is more robust than Otsu thresholding.

Step 3: Lastly, the range of soft tissue intensities (*c*-*d*) is divided by a third threshold *e* to separate dense tissue. This threshold is found using the Otsu algorithm.

The accuracy of this multiple thresholding stage is important, since it affects subsequent stages. We found it can successfully segment dense tissue in all the CT scans.

2.2. Liver localization

Once the dense tissue is segmented from CT image, it can be used to guide liver localization. For this purpose we used our proposed method of liver localization, the method consists of two main components, mean shape model construction and model localization, the detailed steps are in the published paper [30].

The mean shape model of the liver is constructed from ground-truth liver segmentations in training data sets. Model localization itself consists of two sub steps: liver center estimation and model registration. Liver center estimation utilizes the dense tissue segmented from the CT image from the previous stage (multiple thresholding). We used the distance transform to find an approximate liver center, and then to map the shape model to that location inside the target CT scan. When applying the distance transform, the center will be inside the liver, as it is considered the largest singular organ in the human abdomen. We found that this method successfully estimates the liver center in all the CT scans used for evaluation.

However directly placing the mean shape model at the estimated liver center is insufficient. Figure 3(a) shows that the mean shape example, it is not oriented properly and is of incorrect size. Therefore, the mean shape is registered using intensity-based registration with the mutual information similarity metric initialized at the estimated liver centre found from the previous step. Mutual information is utilized as the similarity metric as we found it to robustly register the mean shape to

all datasets in our evaluation. We used two consecutive transformation to perform this registration; first a rigid applied. The rigidly registered mean liver shape is then transformed affinely to better register it to the CT scan. Figure 3(b) shows the mean shape after rigid registration, while Fig. 3(c) shows the result of mean shape localization after applying affine-based registration.

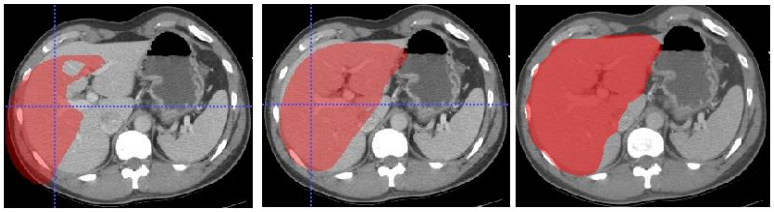

Fig. 3. Shape model localization; (a) at estimated center and after (b) rigid registration and (c) affine registration.

2.3. Liver intensity range estimation: Multiple thresholding within the liver ROI

The aim in this stage is to find an accurate liver intensity range within a specified liver region of interest (ROI). The first step is to construct the ROI, which can be made from intersecting the localized registered mean shape from stage 2.2 (Fig. 3(a)) with the extracted dense tissue from stage 2.1. This helps separate the liver with other neighboring abdominal organs and tissue of similar intensity, as noted by other authors [31].

The second step is to determine the range of liver intensities within the liver ROI. To perform this, we assume that it includes three classes of tissue. The first class consists of tissue with low intensities, which include parts of neighbouring organs such as the gallbladder and surrounding anatomy such as muscles, due to inaccuracies in the ROI construction. The second class consists of tissue with high intensities, which represent tissue with more enhancement from injected contrast such as parts of the kidneys and liver vessels. The third class, with intensities between the first two classes, is considered as actual liver tissue. Hence, multiple thresholding is applied again within the constructed liver ROI. This process is illustrated by Fig. 4.

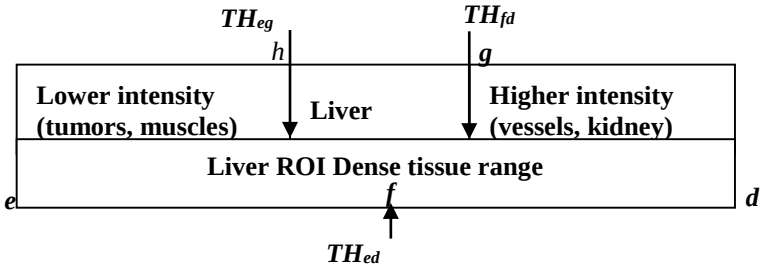

Fig. 4. Multiple thresholding steps within the liver ROI.

As shown in Fig. 4, the following thresholding steps are applied within the range of intensities in the liver ROI (e-d). The thresholds in all three steps are found using the Otsu algorithm.

Step 1: The range (*e*-*d*) is first divided with a threshold *f*. This threshold is only used as a reference point and is not used to define any tissue intensity range.

Step 2: The range (*f*-*d*) is then divided with a second threshold *g*. The range (*g*-*d*) thus is considered to represent tissue with higher intensities cluster, i.e., vessels and parts of kidneys.

Step 3: The lower range of intensities (*e*-*g*) is then divided with a third threshold *h*. The range (*e*-*h*) is then considered lower intensity tissue (gall bladder, tumors, muscles etc.) while the range (*h*-*g*) is considered to represent actual liver tissue.

In some CT images, the liver vessels have high intensity values due to high contrast, which affects the process of intensity analysis inside the constructed liver ROI. In this case, the final threshold h will be too high, which does not reflect the accurate liver intensities threshold. We implemented our approach to detect this situation automatically, as it will cause the ratio of the number of identified liver tissue voxel (with intensities between h-g) to the total number of ROI voxels to be small. We overcome this situation with a different determination of the thresholds in this case. Instead of the process in Fig. 4, we propose that after the initial threshold f, we define a new threshold i, found using GMM with the EM algorithm on the range e-f. This is because in this case, the initial threshold f is high, and therefore the range f-d now represents higher intensity tissue, i.e., vessels. This alternative classification of tissue can be represented by Fig. 5.

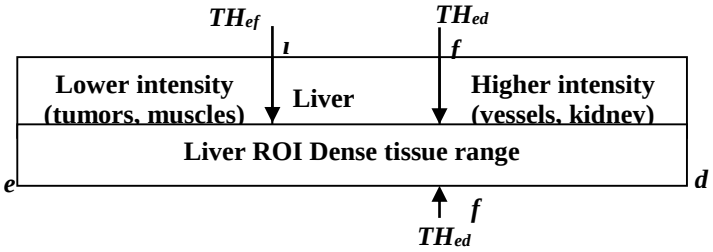

Fig. 5. Alternative classification of tissue within the liver ROI (CT with higher contrast enhancement)

Figure 6 shows an example result of the liver (and other anatomy) determined from this intensity analysis stage.

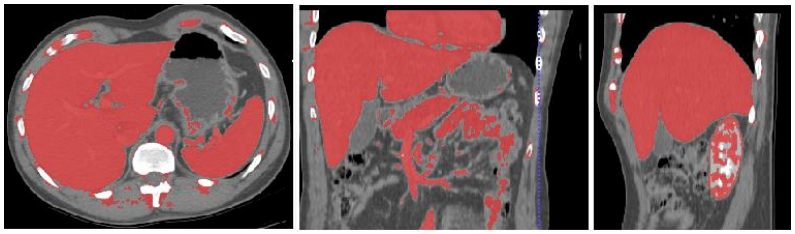

Fig. 6. Example axial, coronal and sagittal slices showing tissue determined from the intensity analysis stage.

This stage is considered the main stage in our approach, since it determines the approximate liver intensity range, and using this range, the subsequent segmentation process using active contours will be constrained to fit to the liver boundary in the CT scan. Therefore, in this approach, the use of the GMM algorithm is optional based on the CT scan. The GMM algorithm proved its superiority over Otsu method to find the correct thresholds, when dealing with high intensity structures (like bones) and when the vessels structure inside the liver ROI has high intensity value. Multiple thresholding proposed in this step succeeded in determining the approximate range of liver intensities in most of CT data sets used in evaluation.

2.4. Level set based localized active contour

In this stage, an active contour method is used to deform an initial mask, i.e., liver segmentation to match more accurately the boundary of the liver in the CT scan. We use a region based level set based active contour, namely that proposed by Chan and Vese [32]. The Chan-Vese energy, Ecv, which is to be minimised, is represented by Eq. (7):

$$E_{CV}[C] = \mu \int_0^{L(C)} ds + \iint_{\Omega_c} (I(x,y) - c_1)^2 dxdy + \iint_{\Omega_c} (I(x,y) - c_2)^2 dxdy \quad (7)$$

Where Ωc represent the interior of the curve C, c1 and c2 are the mean intensities for the interior and the exterior of the curve to be defined in an image I. The first term is the regularization term that minimize the curve length s, and the second term maintains the balancing between the interior and the exterior.

For efficiency, we used localized implementation of this active contour method [33], which only computes the level set function around a certain radius at each point of the contour.

Before applying the localized active contouring method, first, we construct an initial mask, i.e., an initial segmentation of this liver. This initial segmentation of the liver is defined as the intersection of the localized shape model from stage 2 (Subsection 2.2) and the estimated liver intensity range from stage 3 (Subsection 2.3). Thus, tissue from other anatomy such as the kidneys, gallbladder or the surrounding muscles are excluded.

Starting from this initial segmentation of the liver, we apply the localized-contouring algorithm in 2D in all slices and in all three orthogonal planes. We propagate a previously segmented slice as the initial segmentation for a subsequent slice, starting from the center of the liver. We found this method to be better than applying 3D active contours as it better segments the extremities of the liver. The results of the contour deformation is presented in the results section. It is proved that the localized active contour successfully deforms the initial mask to better follow the liver boundaries.

2.5. Post processing

In some cases, the active contour stage above (Subsection 2.4) may extend the mask beyond the liver boundaries, which leads to leakages to surrounding organs. This occurs in some data sets where the surrounding organs have similar intensities, such as the heart and kidneys. In this stage, the aim is to remove the cases of over-

segmentation cases due to deformation leakage to the surrounding organs. These organs generally have higher intensity values compared to liver tissue. They can be identified as the higher intensity cluster from the intensity analysis stage (Subsection 2.3). To define more accurately these clusters, the multiple thresholding stage (Subsection 2.3) is reapplied on the segmentation result of the localized active contour in the previous stage (Subsection 2.4). The aim is to extract a new threshold of the higher intensities, which include voxels belonging to the kidneys and inferior vena cava. Figure 7 shows an example of the extracted higher intensities inside the segmented liver.

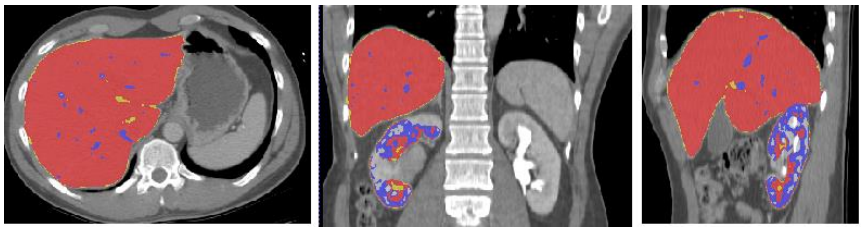

Fig. 7. Example axial, coronal and sagittal slices of the higher intensities tissues identified (blue).

In some cases, the kidney and liver vessels have an intensity range which overlap that of the bones, hence for this stage, the bone intensity range is included is this higher intensity cluster. Additional morphological opening, closing and region filling operations helped in removing the small extensions to the surrounding structures like ribs and top part of kidney, and as a result refine and enhance the segmented liver.

3. Results and Discussion

3.1. Validation data

The method has been validated on two publicly available data sets, the SLIVER07 dataset [27] and the 3D-IRCAD dataset. Both datasets have the standard CT slice dimensions of 512 × 512 pixels. The SLIVER07 dataset contains 30 contrast enhanced CT images from different patients respectively. The ground truth segmentation for 20 images are provided, and we only used these in our evaluation. The data sets are challenging and most of them are pathologic. The in plane resolution ranges between 0.58 to 0.81 mm. The number of slices for each patient varies between 64-394 slices; with slice spacing ranging between 0.7 to 5.0 mm.

The 3D-IRCAD dataset on the other hand are more challenging than the SLIVER07 dataset as they have more pathologic cases. This dataset contain 20 images with in-plane resolution ranging between 0.56 to 0.86 mm. The number of slices for each patient varies between 148-260 slices; with inter slice spacing ranging from 1.0 to 4.0 mm.

3.2. Segmentation results and discussion

Figure 8 shows selected axial slices of the results for the three main stages (localized shape model, pre-active contour mask, final segmentation) in the proposed methodology for three different images, two from SLIVER07 (the first and second

rows) and one from 3D-IRCAD (third row). These results (in blue) are compared to the ground truth segmentations (red). The first column (a) shows the localized shape model, the second column (b) shows the mask for the localized active contour algorithm, the third column (c) represent the final result of segmentation after the post-processing stage. It can be seen that the liver organ is successfully extracted from the images by the proposed method and are comparable to the ground truth segmentation (red). We choose selected these three cases amongst the 40 images that we evaluated upon to highlight the strong results of our approach as well as limitations, as discussed below.

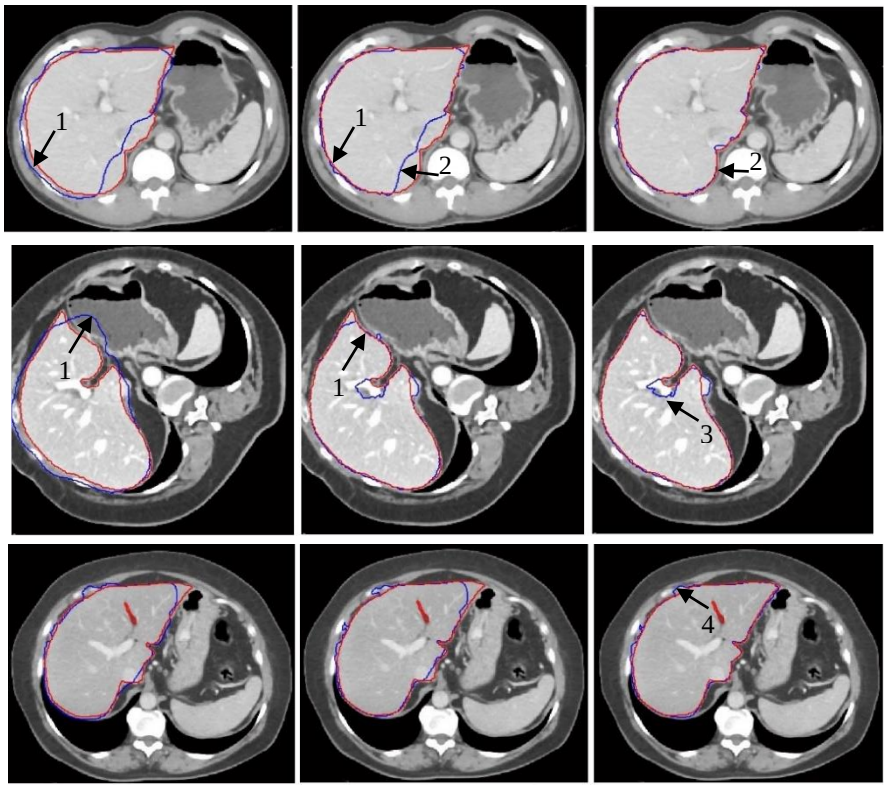

Fig. 8. Segmentation method steps output (images from SLIVER07 for first and second rows, and from 3D-IRCAD for third row): (a) localized shape model, (b) pre-active contour mask, and (c) the final segmentation (blue), compared to ground truth segmentation (red).

The boundaries marked by number 1 in the first two data sets, show how the proposed method, using the liver intensity range estimation stage (Subsection 2.3), succeeds to improve the localized mean liver shape (first column) to better follow liver boundaries in forming the pre-active contour mask (second column).

The boundary marked by number 2 in the first data set shows that the localized active contour stage succeeds in deforming the mask contour to refine the liver

boundary in the CT image. However, in some data sets intensity similarity either side of the liver boundaries due and low contrast cause some leaks to surrounding tissue.

The second data set (row 2) has an under-segmentation case marked by number 3, this is part of the portal vein when it crosses the boundary of the liver. Vessels have high intensity values, which make them outside the estimated liver intensity range (Subsection 2.3) and not be considered as part of the liver in our approach. However, other vessels that are located inside the liver region are included even though they have high intensity values.

An over-segmentation case is present in the third data set marked by number 4. This case shows an example of unclear liver boundary due to low contrast, which may lead to the active contour stage to deform the mask to the neighboring tissues, which have similar intensities.

In most of data sets, the neighboring organs like kidney and heart, are already excluded, since their intensity values are not located within the estimated liver intensity range and hence are excluded during the localized active contouring step. However, some of the over-segmentation cases happen when there are unclear boundaries between the liver and surrounding organs. Here, the post-processing stage removes these parts of neighboring organs such as the kidneys or heart which are erroneously included in the segmentation at the active contour stage.

Figure 9 shows selected sagittal slices for two data sets (per row), to highlight the post-processing stage in the proposed method. Column (a) shows the result after applying localized active contour to deform the pre-contour mask while column (b) shows the extraction of kidney and other surrounding tissues according to the method proposed in the post-processing stage in Subsection 3.5. Column (c) shows the final segmentation result after removing the over-segmented parts.

Results in Fig. 9 show that the liver is delineated accurately from the surrounding organs such as the heart, kidney and spleen, which have similar intensity values. There are only a few under or over-segmentation cases due to the extension by the localized contouring stage. The proposed segmentation method is independent on the shape, size, position and intensity distribution of the liver. Furthermore, the method is validated on challenging datasets (40 patients), where the size of the liver is different from one patient to another, and have irregular liver shapes.

With our approach, we ignore that tumors impose a challenge, as they have low intensity values compared to the liver parenchyma. These intensities do not appear within the estimated liver intensity range (Subsection 2.3), and this affects the segmentation result. Some data sets have tumors with different sizes and may appear at different locations, inside the liver or at the border of the liver. With tumors located on the surface of the liver, deformation of the contour to the actual liver boundary is affected. However, in general these cases do not significantly affect our results when compared to other works which are discussed below.

To quantitatively assess and evaluate the proposed liver segmentation method, a group of performance measures is used. We quantitatively compare the output of the proposed segmentation method with ground truth segmentation of each image. Three metrics are used to evaluate the results of the proposed segmentation method, the volume overlap error (VOE), the Dice coefficient (Dice) and the Absolute Relative Volume Difference (ARVD). In Eqs. (3)-(5) below, |A| denotes the number of voxels in a segmentation

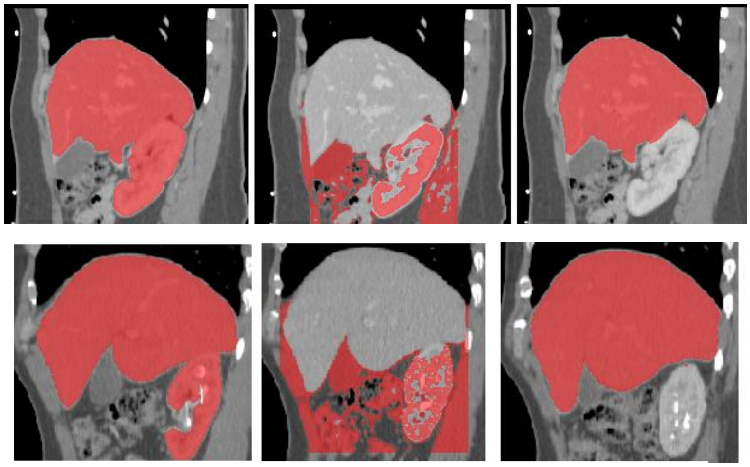

(a) (b) (c)

Fig. 9. Selected sagittal slices showing (a) pre-refinement (before kidney extraction), (b) kidney extraction (intensity range estimation), and (c) segmentation after removing over segmented parts.

The Volume Overlap Error (VOE) metric is related to the Jaccard index, which is considered as another common metric to measure volumetric overlap accuracy. The VOE, is defined by Eq. (8), where (A) denotes the segmentation result by the proposed method and (B) is the ground truth data segmentation.

$$VOE\ (A,B) = 1 - |A \cap B| / |A \cup B| \tag{8}$$

The second performance measure is the Absolute Relative Volume Difference (ARVD), defined by Eq. (9). It measures the difference in volume between the segmented liver and its corresponding ground truth. It reflects the amount of under and over segmentations. However this metric only compares volume, hence a value of zero does not necessarily reflect a perfect segmentation.

$$ARVD\,(A,B) = (|A| - |B|) / |B| \tag{9}$$

The third measure used is the Dice coefficient (DSC), defined by Eq. (10). It is another overlap measure that compute the ratio between the correctly segmented liver voxels (intersection) with respect to the total number of voxels of the segmentation output and the ground truth.

$$Dice\,(A,B) = 2*|A \cap B| / (|A| + |B|) \tag{10}$$

Table 1 presents the quantitative results of the proposed segmentation method. The average VOE are 7.07±1.56% and 10.31±4.0%, the ARVD values are 2.2% and 4.4% , and the Dice coefficient values are 96.32% and 94.51 %, for the SLIVER and 3D-IRCAD data sets, respectively.

Additionally, Table 1 shows the quantitative comparison between the proposed method with previous techniques [5, 9, 10, 16, 19, 34, 37]. Type indicates if the method is fully or semi-automatic. The table shows the evaluation of the previously proposed methods applied on the SLIVERO7, 3D-IRCAD and private data sets.

The method results are comparable and reside within the range of other results. The step of intensity analysis inside the liver ROI, enables the method to find the accurate estimation of the liver intensity range, compared to other techniques [5, 9, 10] that used few slices to extract the liver intensity range, which does not reflect the accurate liver characteristics. The proposed method showed superior performance over other intensity-based methods, besides that, most of them are not fully automatic and need the user intervention. It should be noted though that some of these methods used different data sets to validate their algorithms.

The results in Table 1 show that the proposed method succeeded on segmenting the liver correctly with high accuracy (VOE of 7-10 %), which is considered a good indicator for clinical applications. This help to make an accurate volume calculation for each patient, which can be used for example to perform proper preoperative planning of risks during resection surgery. This is an advantage over other techniques that depend on a training phase to segment the targets CT scans, such as statistical shape model based methods and learning based approaches [21, 34]. These methods would fail in cases where there are large deviations from a presumed normal shape of the liver. These methods require to large ground truth training data sets to cover the high liver variability, which is not always available. These methods may fail to model all liver shapes accurately; especially with those that have abnormalities or resected livers.

Table 1. Comparison with previous methods evaluated with different datasets.

Method	Type	ARVD %	VOE %	DSC %
Erdt et al. [21] **(SLIVER07)**	Auto	1.28	7.54±1.18	-
Erdt et al. [21] **(IRCAD)**	Auto	1.5	10.34±3.11	-
Kirschner [34] **SLIVER07)**	Auto	1.49	5.82	97
Kirschner [34] **(IRCAD)**	Auto	3.62	9.52	95
Li et al. [17]**(SLIVER07)**	Auto	1.18	6.24±1.52	-
Li et al. [17] **(IRCAD)**	Auto	0.07	9.15±1.44	-
Linguraru et al. [35]	Auto	2.6	8	95.8
Rusko et al. [9]	Auto	4.3	10.7	-
Chung and Delingette [36] **(IRCAD)**	Auto	5.66	12.99	-
Foruzan et al.[5]	Semi	4.06	12.51	93.3
Goryawala et al. [10]	Semi	2.78	14.81	92
Platero and Tobar [16]	Auto	0.5	7.6	-
Oliveira et al.[37]	Semi	2.19	7.35	-
Christ et al. [26] **(IRCAD)**	Auto	1.4	10.7	94.3
Proposed Method (SLIVER07)	Auto	2.2	7.07±1.56	96.32
Proposed Method (IRCAD)	Auto	4.4	10.31±4.0	94.51

4. Conclusion

The proposed method is based on liver intensity range estimation and level set localized active contours. The liver intensity range estimation is applied in an initial liver ROI defined by a localized mean shape model. Accurate estimation of the liver intensity range is used to form an accurate pre-contour mask, which is then deformed using localized active contours. The proposed post-processing step trim leakage to surrounding organs and enhanced the final segmentation output. The method outperforms many of recent works, and is comparable to the state of the art. The validation results demonstrate the effectiveness of the proposed method.

Acknowledgements

This research is supported by the Malaysian Ministry of Higher Education and Universiti Kebangsaan Malaysia under grant no. GUP-2014-066.

Nomenclatures

E_{cv}	Chan-Vese energy, hu
HU	Intensity Hounsfield units
T_g	Global threshold, hu
w	Class probability

Greek Symbols

$\boldsymbol{\mu}_k$	Gaussian density mean, hu
π_k	Gaussian density mixing coefficient, hu
$\sum_k$	Gaussian density covariance, hu
σ^2	Class Variance, hu.
Ω_c	Chan-Vese interior of the curve C

Abbreviations

2D	Two dimensions
3D	Three dimensions
ARVD	Absolute Relative Volume Difference
CT	Computed tomography
EM	Expectation maximization
FCN	fully Conventional Neural Networks
GMM	Gaussian mixture model
PCA	Principal component analysis
ROI	Region of interest
SSM	Statistical shape model
VOE	Volume overlap error
XCAT	Extended cardiac-torso

References

1. Priyadarsini, S.; and Selvathi, D. (2012). Survey on segmentation of liver from CT images. *Proceedings of 2012 IEEE International Conference on Advanced Communication Control and Computing Technologies, (ICACCCT).* Ramanathapuram, India, 234-238.

2. Sharma, N.; and Aggarwal, L.M. (2010). Automated medical image segmentation techniques. *Journal of Medical Physics*, 35(1), 3-14.
3. Pamulapati, V.; Venkatesan, A.; Wood, B.J.; and Linguraru, M.G. (2012). Liver segmental anatomy and analysis from vessel and tumor segmentation via optimized graph cuts. *Abdominal Imaging, Computational and Clinical Applications*, 189-197.
4. Boas, F.E.; and Fleischmann, D. (2012). CT artifacts: Causes and reduction techniques. *Imaging in Medicine*, 4(2), 229-240.
5. Foruzan, A.H.; Chen, Y.-W.; Zoroofi, R.A.; Furukawa, A.; Sato, Y.; Masatoshi, H.; and Tomiyama, N. (2013). Segmentation of liver in low-contrast images using K-means clustering and geodesic active contour algorithms. *IEICE Transactions on Information and Systems*, E96-D(4), 798-807.
6. Campadelli, P.; Casiraghi, E.; and Esposito, A. (2009). Liver segmentation from computed tomography scans: A survey and a new algorithm. *Artificial Intelligence in Medicine*, 45(2-3), 185-196.
7. Luo, S.; Li, X.; and Li, J. (2014). Review on the methods of automatic liver segmentation from abdominal images. *Journal of Computer and Communications*, 2(2), 1-7.
8. Mharib, A.M.; Ramli, A.R.; Mashohor, S.; and Mahmood, R.B. (2012). Survey on liver CT image segmentation methods. *Artificial Intelligence Review*, 37(2), 83-95.
9. Rusko, L.; Bekes, G.; and Fidrich, M. (2007). Fully automatic liver segmentation for contrast-enhanced CT images. *Proceedings of the International Conference on Medical Image Computing and Computer-Assisted Intervention.* Brisbane, Australia, 143-150.
10. Goryawala, M.; Gulec, S.; Bhatt, R.; McGoron, A.J.; and Adjouadi, M. (2014). A low-interaction automatic 3D liver segmentation method using computed tomography for selective internal radiation therapy. *BioMed Research International*, Article ID 198015, 12 pages.
11. Altarawneh, N.M.; Luo, S.; Regan, B.; and Sun, C. (2015). A modified distance regularized level set model for liver segmentation from CT images. *An International Journal (SIPIJ)*, 6(1), 11 pages.
12. Foruzan, A.H.; Chen, Y.-W.; Zoroofi, R.A.; Furukawa, A.; Sato, Y.; and Hori, M. (2009). Multi-mode narrow-band thresholding with application in liver segmentation from low-contrast CT images. *Proceedings of the 5th International Conference on Intelligent Information Hiding and Multimedia Signal Processing*. Kyoto, Japan, 1293-1296.
13. Kumar, S.S.; Moni, R.S.; and Rajeesh, J. (2013). Automatic liver and lesion segmentation: A primary step in diagnosis of liver diseases. *Signal, Image and Video Processing*, 7(1), 163-172.
14. Wang, Q.; Song, X.; and Jiang, Z. (2013). An improved image segmentation method using three-dimensional region growing algorithm. *Proceedings of the International Conference on Information Science and Computer Applications (ISCA)*. Hu Nan, China, 148-152.
15. Chen, Y.; Wang, Z.; Zhao, W.; and Yang, X. (2009). Liver segmentation from CT images based on region growing method. *Proceedings of the 3rd*

International Conference on Bioinformatics and Biomedical Engineering. Beijing, China, 1-4.

16. Platero, C.; and Tobar, M.C. (2014). A multiatlas segmentation using graph cuts with applications to liver segmentation in CT scans. *Computational and Mathematical Methods in Medicine*, Article ID 182909, 16 pages.
17. Li, G.; Chen, X.; Shi, F.; Zhu, W.; Tian, J.; and Xiang, D. (2015). Automatic Liver Segmentation Based on Shape Constraints and Deformable Graph Cut in CT Images. *IEEE Transactions on Image Processing*, 24(12), 5315-5329.
18. Wu, W.-W.; Wu, S.-C.; Zhang, R.; Zhou, Z-H; and Zhang, Y.-H. (2016). Fast graph cuts based liver and tumor segmentation on volumetric CT images. *Proceedings of the Joint International Conference on Service Science, Management and Engineering (SSME).* Wuhan, China, 1-5.
19. Liao, M.; Zhao, Y-q; Liu, X.-y.; Zeng, Y.-z.; Zou, B.-j.; Wang, X.-f.; and Shih, F.Y. (2017). Automatic liver segmentation from abdominal CT volumes using graph cuts and border marching. *Computer Methods and Programs in Biomedicine* , 143, 1-12.
20. Kainmuller, D.; Lange, T.; and Lamecker, H. (2007). Shape constrained automatic segmentation of the liver based on a heuristic intensity model. *Proceedings of the MICCAI Workshop on 3D Segmentation in the Clinic: A Grand Challenge.* Brisbane, Australia, 109-116.
21. Erdt, M.; Steger, S.; Kirschner, M.; and Wesarg, S. (2010). Fast automatic liver segmentation combining learned shape priors with observed shape deviation (CBMS). *Proceedings of the IEEE Symposium on Computer-Based Medical Systems*. Perth, Australia, 249-254.
22. Heimann, T.; and Delingette, H. (2011). Model-based segmentation. *Biomedical Image Processing*, 279-303.
23. Heimann, T.; and Meinzer, H.-P. (2009). Statistical shape models for 3D medical image segmentation: A review. *Medical Image Analysis*, 13(4), 543-563.
24. Li, X.; Huang, C.; Jia, F.; Li, Z.; Fang, C.; and Fan, Y. (2014). Automatic liver segmentation using statistical prior models and free-form deformation. *Medical Computer Vision: Algorithm for Big Data*, 181-188.
25. Linguraru, M.G.; Sandberg, J.K.; Li, Z.; Shah, F.; and Summers, R.M. (2010). Automated segmentation and quantification of liver and spleen from CT images using normalized probabilistic atlases and enhancement estimation. *Medical Physics*, 37(2), 771-783.
26. Christ, P.F.; Ettlinger, F.; Grun, F.; Elshaera, M.E.A.; Lipkova, J.; Schlecht, S.; Ahmaddy, F.; Tatavarty, S.; Bickel, M.; Bilic, P.; Rempfler, M.; Hofmann, F.; Anastasi, M.D.; Ahmadi, S.-A.; Kaissis, G.; Holch, J.; Sommer, W.; Braren, R.; Heinemann, V.; and Menze, B. (2017). Automatic liver and tumor segmentation of CT and MRI volumes using cascaded fully convolutional neural networks. *Computer Vision and Pattern Recognition*, 1-20.
27. Heimann, T.; Ginneken, B.v.; Styner, M.A.; Arzhaeva, Y.; Aurich, V.; Bauer, C.; Beck, A.; Becker, C.; Beichel, R.; Bekes, G.; Bello, F.; Binnig, G.; Bischof, H.; Bornik, A.; Cashman, P.M.M.; Chi, Y.; Cordova, A.; Dawant, B.M.; Fidrich, M.; Furst, J.D.; Furukawa, D.; Grenacher, L.; Hornegger, J.; Kainmuller, D.; Kitney, R.I.; Kobatake, H.; Lamecker, H.; Lange, T.; Lee, J.; Lennon, B. (2009). Comparison and evaluation of methods for liver

segmentation from CT datasets. *IEEE Transactions on Medical Imaging*, 28(8), 1251-1265.

28. Otsu, N. (1975). A threshold selection method from gray-level histograms. *IEEE Transactions on Systems, Mans, and Cybernatics*, 9(1), 62-66.
29. Bishop, C.M. (2006). Pattern recognition and machine learning. *Springer*.
30. Irr, O.I.A.; and Rahni, A.A.A. (2015). Automatic volumetric localization of the liver in abdominal CT scans using low level processing and shape priors. *Proceedings of the IEEE International Conference on Signal and Image Processing Applications (ICSIPA)*. Kuala Lumpur, 434-438.
31. Foruzan, A.H.; Zoroofi, R.A.; Hori, M.; and Sato, Y. (2009). A knowledge-based technique for liver segmentation in CT data. *Computerized Medical Imaging and Graphics*, 33(8), 567-587.
32. Chan, T.F.; and Vese, L.A. (2001). Active contours without edges. *IEEE Transactions on Image Processing*, 10(2), 266-277.
33. Lankton, S.; and Tannenbaum, A. (2008). Localizing region-based active contours. *IEEE Transactions on Image Processing*, 17(11), 2029-2039.
34. Kirschner, M. (2013). *The probabilistic active shape model : From model construction to flexible medical image segmentation*. Ph.D. Thesis. Technical University Darmstadt, Deutschland.
35. Linguraru, M.G.; Sandberg, J.K.; Li, Z.; Shah, F.; and Summers, R.M. (2010). Automated segmentation and quantification of liver and spleen from CT images using normalized probabilistic atlases and enhancement estimation. *Medical Physics*, 37(2), 771-783.
36. Chung, F.; and Delingette, H. (2013). Regional appearance modeling based on the clustering of intensity profiles. *Computer Vision and Image Understanding*, 117(6), 705-717.
37. Oliveira, D.A.; Feitosa, R.Q.; and Correia, M.M. (2011). Segmentation of liver, its vessels and lesions from CT images for surgical planning. *Biomedical Engineering Online*, 10(1), 23 pages.